Finite Element Analysis of an External Rotor Permanent Magnet Synchronous Machine with Star- and Delta-Connected Tooth Coil Windings

Erich Schmidt, Marko Sušić, Andreas Eilenberger
Institute of Electrical Drives and Machines, Vienna University of Technology, Vienna, Austria
erich.schmidt@tuwien.ac.at

***Abstract* – The permanent magnet synchronous machine with an external rotor is the most important device for high performance electrical drive systems in particular for hybrid electric vehicles. The paper discusses finite element analyses of such a machine with concentrated tooth coils in terms of a comparison of both Y- and Δ-connected stator windings. As the evolved electromagnetic torque is one of the most important design parameter, various ratios of tooth width and slot pitch are analyzed with the two connections of the stator winding. On the other hand, the phase voltages for various operating conditions are compared between both Y- and Δ-connected stator windings.**

***Keywords* – Permanent magnet synchronous machine, Tooth coil windings, Finite element analysis**

I. Introduction

THE permanent magnet excited synchronous machine (PMSM) with fractional slot stator windings using tooth coil technology provides an increased torque capability due to a more compact construction [1]–[4]. Thus, the PMSM in particular with an external rotor is the most important device for high performance electrical drive systems such as wheel hub drives of electric driven vehicles. For such an application, the torque ripple shows high significance and should be as small as possible [5], [6].

The paper discusses finite element analyses of a PMSM with an external rotor in terms of a comparison of both Y- and Δ-connected fractional slot stator windings with tooth coils. Since both connections will provide different spectra for magnetic flux and magneto motive force, they will significantly influence the machine parameters such as phase voltages and electromagnetic torque. In order to validate the results obtained from the numerical analyses, they are successfully compared with measurement results.

II. Finite Element Modelling

Table I lists the main data of the investigated PMSM with an external rotor. According to these geometry data, we have the winding data as listed in Table II. Consequently, the machine can be equipped with a single-layer fractional slot tooth coil winding of first kind.

TABLE I
Main Data of the Permanent Magnet Synchronous Machine

Number of phases	m	3	
Number of poles	$2p$	30	
Number of slots	Q	36	
Airgap length		2	mm
Inner Stator Diameter		200	mm
Outer Rotor Diameter		400	mm
Remanent flux density		1.30	T
Coercive field strength		985.25	kA/m

TABLE II
Winding Data of the Permanent Magnet Synchronous Machine

Number of slots per pole and phase	q	$\frac{z}{n}$	$\frac{2}{5}$
Number of base windings	t	$\frac{p}{n}$	3
Number of slots per base winding	Q^*	$\frac{Q}{t}$	12
Number of poles per base winding	$2p^*$	$\frac{2p}{t}$	10
Winding pitch	σ	$\frac{1}{mq}$	$\frac{5}{6}$

As shown in Fig. 1, the smallest necessary section of the entire machine for the finite element model consists of only five poles representing a half of a base winding. To reflect the required periodicity of the magnetic field with the unknown degrees of freedom of the magnetic vector potential, anti-periodic boundary conditions are utilized at the boundaries being five pole pitches apart.

All analyses utilize fully independent models of rotor and stator denoted as Ω_{rt} and Ω_{st} which are described with their own matrix equations

$$\left(\mathbf{C}_m \frac{d}{dt} + \mathbf{K}_m\right)\mathbf{U}_m + \mathbf{G}_m = \mathbf{P}_m \ , \ \ m = \{st, rt\} \ . \quad (1)$$

Both model parts are constructed with an equidistant discretization in circumferential direction along

978-1-4244-4175-4/10/$25.00 ©2010 IEEE

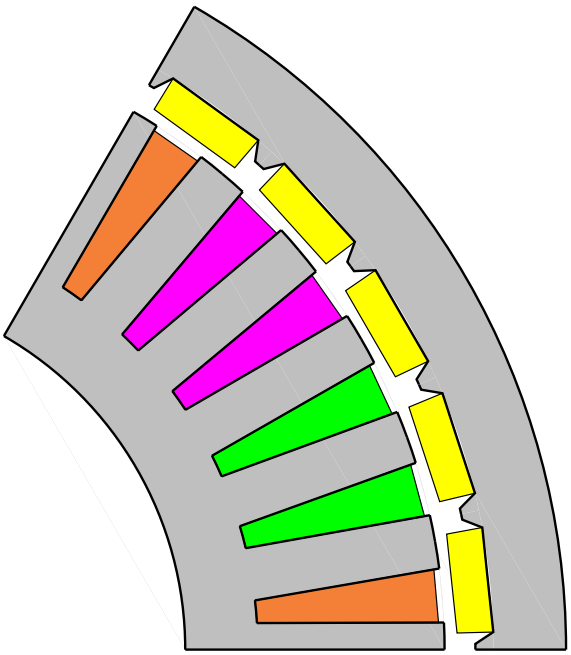

Fig. 1: Cross section of permanent magnet synchronous machine with an external rotor

the sliding surface interface Γ_{sl} within the air-gap as shown in Fig. 2 [7], [8]. In dependence on the angular rotor position, these two model parts are coupled together by floating multipoint boundary conditions

$$\mathbf{U}_{rt,e} = \mathbf{E}_k\,\mathbf{U}_{st,e} \ , \quad \mathbf{G}_{st,e} = -\mathbf{E}_k^T\,\mathbf{G}_{rt,e} \ . \tag{2}$$

for their exterior unknown degrees of freedom along the boundaries Γ_{rt} and Γ_{st} on the sliding surface interface Γ_{sl} [8]–[11]. Consequently, any remeshing of the air-gap region is avoided yielding an identical quality of the numerical results for the analyses of subsequent angular rotor positions [10], [11].

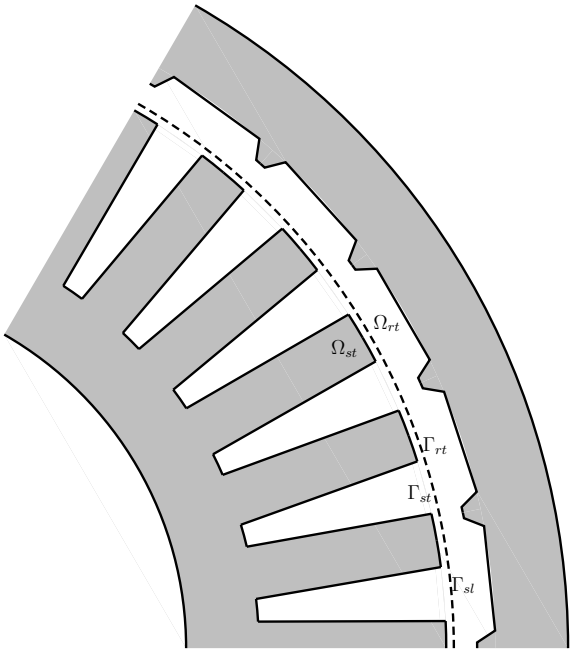

Fig. 2: Domain parts with the sliding surface approach

III. Space Vector Calculus

The various analyses are based on the field oriented control of the PMSM by using stator current and stator flux space vectors. In the dq rotor fixed reference frame [12], [13], the normalized stator current and stator flux space vectors are given by

$$\underline{i}_{S,dq} = i_S\,e^{\jmath\beta} \ = i_d + \jmath\, i_q \ , \tag{3}$$

$$\underline{\psi}_{S,dq} = \psi_S\,e^{\jmath\vartheta} = \psi_d + \jmath\,\psi_q \ , \tag{4}$$

where β,ϑ are the stator current angle and the stator flux angle, respectively.

In order to inject the stator currents in the $\alpha\beta$ stator fixed reference frame of the finite element model, the stator current and stator flux space vectors are transformed as given by

$$\underline{i}_{S,\alpha\beta} = \underline{i}_{S,dq}\,e^{\jmath\gamma} \ , \tag{5}$$

$$\underline{\psi}_{S,\alpha\beta} = \underline{\psi}_{S,dq}\,e^{\jmath\gamma} \ , \tag{6}$$

where γ denotes the electric angular rotor position.

In case of a Y-connected stator winding, any zero sequence stator currents are impossible. Therefore, the stator currents are directly deduced from

$$i_{S1} = \mathrm{Re}\big(\underline{i}_{S,\alpha\beta}\big) \ , \tag{7a}$$

$$i_{S2} = \mathrm{Re}\big(\underline{i}_{S,\alpha\beta}\ \mathrm{e}^{-\jmath 2\pi/3}\big) \ , \tag{7b}$$

$$i_{S3} = \mathrm{Re}\big(\underline{i}_{S,\alpha\beta}\ \mathrm{e}^{-\jmath 4\pi/3}\big) \ . \tag{7c}$$

On the other hand in case of a Δ-connected stator winding, there is an unknown zero sequence current i_0 with all phases. Therefore, the stator currents are now obtained from

$$i_{S1} = i_0 + \mathrm{Re}\big(\underline{i}_{S,\alpha\beta}\big) \ , \tag{8a}$$

$$i_{S2} = i_0 + \mathrm{Re}\big(\underline{i}_{S,\alpha\beta}\ \mathrm{e}^{-\jmath 2\pi/3}\big) \ , \tag{8b}$$

$$i_{S3} = i_0 + \mathrm{Re}\big(\underline{i}_{S,\alpha\beta}\ \mathrm{e}^{-\jmath 4\pi/3}\big) \ . \tag{8c}$$

The unknown zero sequence current i_0 has to be determined iteratively for each angular rotor position with all operating conditions according to the vanishing sum $u_{S1} + u_{S2} + u_{S3} = 0$ of the three phase voltages.

IV. Analysis Results

A. Comparison with Measurements

Fig. 3 and Fig. 4 depict no-load phase voltages and zero sequence currents of both finite element analysis and measurements for the initial design with the Δ-connected stator winding for the speed of 668 rpm. Obviously, there is a very good agreement between numerical analysis and measurement results.

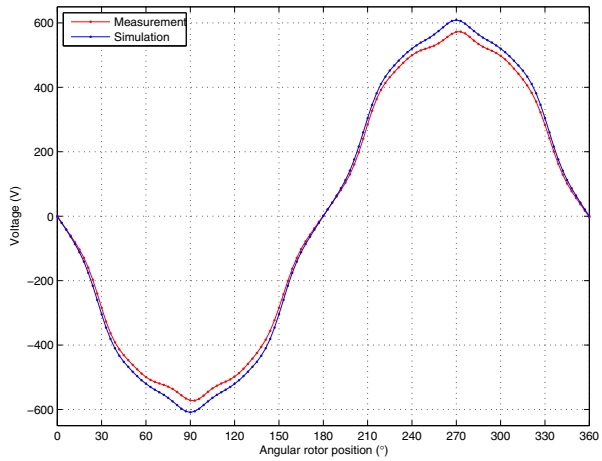

Fig. 3: No-load voltage of the initial design with a Δ-connected stator winding, numerical analysis and measurement results

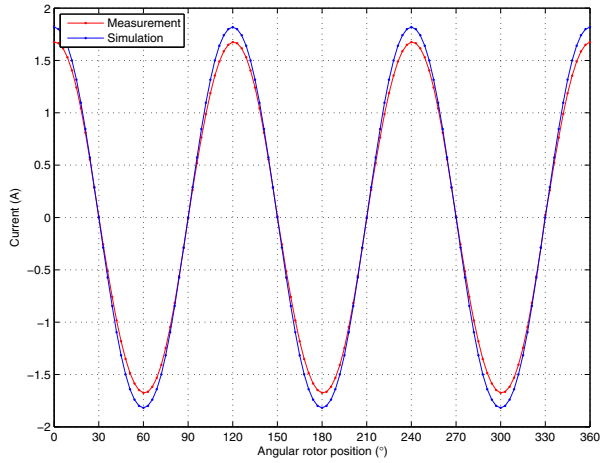

Fig. 4: No-load zero sequence current of the initial design with a Δ-connected stator winding, numerical analysis and measurement results

Additionally, Fig. 5 depicts the average value of the load torque with the initial design in dependence on

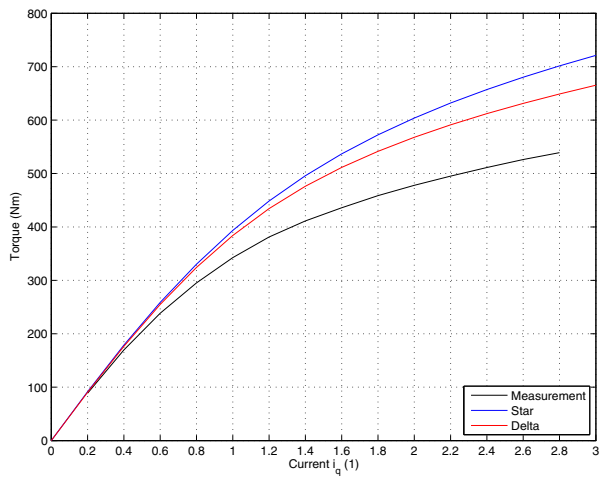

Fig. 5: Load torque of the initial design, Y-connected and Δ-connected stator winding as well as measurement results

the quadrature axis current. The numerical results are shown for both Y-connected and Δ-connected stator windings while the measurement results are obtained from the initial design with a Δ-connected stator winding. There is a good agreement with stator currents in the range up to rated current loads but increasing deviations with larger current loads. They arise from stray field portions in the axial direction in particular with the permanent magnets of the rotor.

B. No-Load Voltages

Fig. 6 and Fig. 7 depict the no-load voltages of one phase with various ratios b_t/τ_s of tooth width and slot pitch and all three phases with the initial design for the speed of 320 rpm for both Y- and Δ-connected stator windings. Accordingly, Table III and Table IV list the magnitudes of the significant harmonics in dependence on the ratio b_t/τ_s.

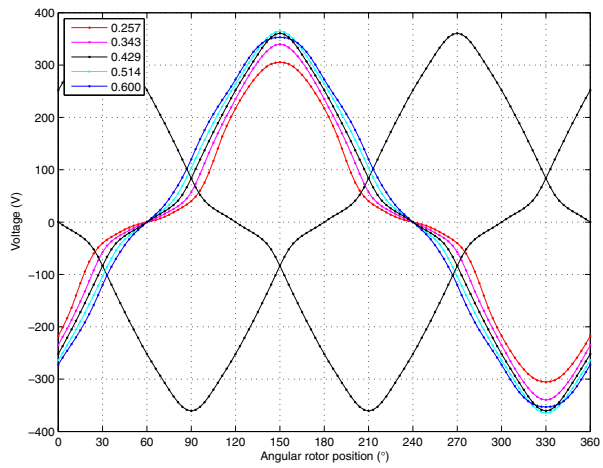

Fig. 6: No-load voltages with various ratios b_t/τ_s of tooth width and slot pitch, Y-connected stator winding

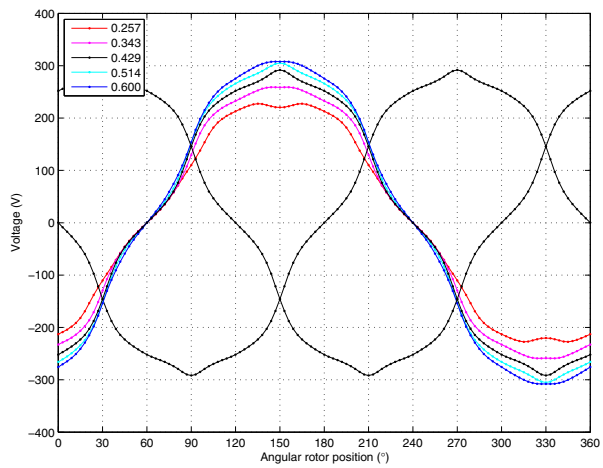

Fig. 7: No-load voltages with various ratios b_t/τ_s of tooth width and slot pitch, Δ-connected stator winding

In comparison of the Y- and Δ-connected stator windings, the latter generates a smaller fundamental

TABLE III
No-load Voltage Harmonics (Magnitudes) with Various Ratios of Tooth Width and Slot Pitch, Y-connected Stator Winding

	Ratio	Voltage (V)				
	b_t/τ_s	1st order	3rd order	5th order	7th order	9th order
	0.257	239.9	73.0	4.1	6.8	3.0
	0.300	255.9	71.7	4.7	2.6	4.8
	0.343	270.1	69.0	4.4	1.3	4.9
	0.386	282.3	65.3	3.7	4.1	4.3
(ID)	0.429	292.6	61.2	3.3	6.0	3.6
	0.471	301.0	56.7	3.4	7.1	2.7
	0.514	307.9	51.4	3.9	7.4	1.6
	0.557	313.5	45.4	4.6	7.0	0.2
	0.600	317.9	38.5	5.4	6.0	1.4

TABLE IV
No-load Voltage Harmonics (Magnitudes) with Various Ratios of Tooth Width and Slot Pitch, Δ-connected Stator Winding

	Ratio	Voltage (V)				
	b_t/τ_s	1st order	3rd order	5th order	7th order	9th order
	0.257	236.3	0.0	14.5	1.6	0.0
	0.300	252.1	0.0	14.6	6.3	0.0
	0.343	266.2	0.0	14.7	10.4	0.0
	0.386	278.5	0.0	14.7	13.3	0.0
(ID)	0.429	288.8	0.0	14.7	14.5	0.0
	0.471	297.4	0.0	14.7	14.4	0.0
	0.514	304.5	0.0	14.9	13.4	0.0
	0.557	310.4	0.0	15.0	11.9	0.0
	0.600	315.3	0.0	14.8	10.0	0.0

harmonic with all ratios b_t/τ_s. Due to the high level of saturation, the no-load voltages contain a significant third harmonic with all design variations in case of the Y-connected stator winding. On the other hand, there is no third harmonic in case of the Δ-connected stator winding. Moreover, the fifth and seventh harmonics are higher with the Δ-connected stator winding than with the Y-connected stator winding.

C. Electromagnetic Torque

As mentioned above, a cogging torque as small as possible is the most important criterion for a drive system of an electric vehicle. Fig. 8 and Fig. 9 as well as Fig. 10 and Fig. 11 depict cogging and load torque with various ratios b_t/τ_s of tooth width and slot pitch for both Y- and Δ-connected stator windings. Accordingly, Table V and Table VI lists the magnitudes of the significant harmonics in dependence on the ratio b_t/τ_s.

In comparison of the Y- and Δ-connected stator windings, the first one shows harmonic components of the cogging torque according to the least common multiple of the number of slots and the number of poles as well as multiples,

$$\nu = \frac{g}{p}\ \mathrm{lcm}\big(Q, 2p\big) = 12g \ , \quad g \in \mathcal{N} \ . \tag{9}$$

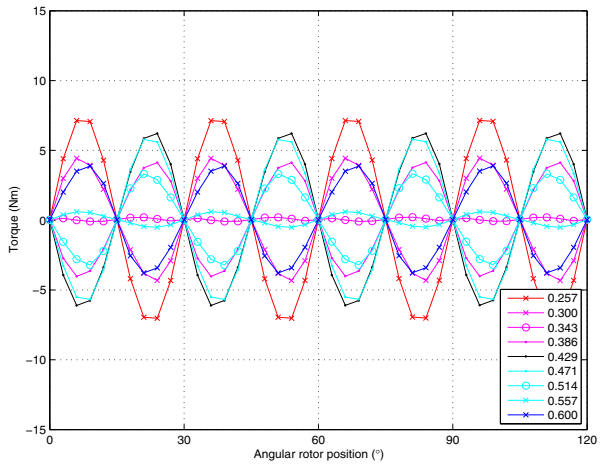

Fig. 8: Cogging torque with various ratios b_t/τ_s of tooth width and slot pitch, Y-connected stator winding

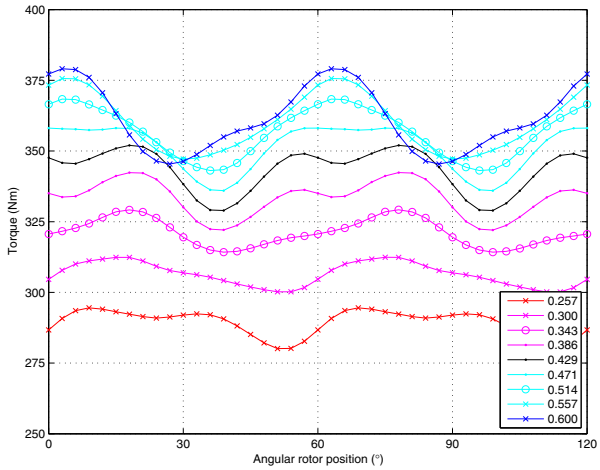

Fig. 9: Load torque with various ratios b_t/τ_s of tooth width and slot pitch, $\underline{i}_{S,dq} = \jmath$, Y-connected stator winding

On the other hand with the latter one, there are harmonic components of orders $6g$, $g \in \mathcal{N}$, and in particular a noticeable sixth harmonic component in the cogging torque resulting from the zero sequence current in the three phases.

The Δ-connected stator winding generates a smaller mean value of the load torque in case of an identical stator current injection $\underline{i}_{S,dq} = \jmath$ and simultaneously a higher cogging torque with all ratios b_t/τ_s.

With both connections, two design variations yield a significantly smaller 12th harmonic component in the cogging torque than the initial design (ID). With respect to a lower saturation level, the higher value of the ratio b_t/τ_s will be preferred.

D. Comparison between Y- and Δ-Connection

In summary, the Y-connected stator winding, in particular due to a high third harmonic, will generate higher iron losses than the Δ-connected stator winding. On the other hand, the zero sequence current of the Δ-

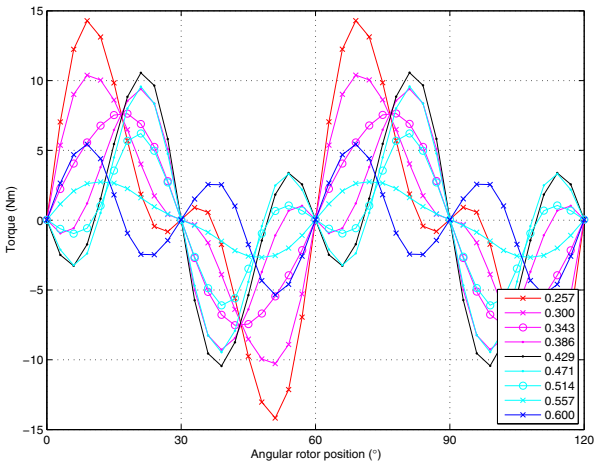

Fig. 10: Cogging torque with various ratios b_t/τ_s of tooth width and slot pitch, Δ-connected stator winding

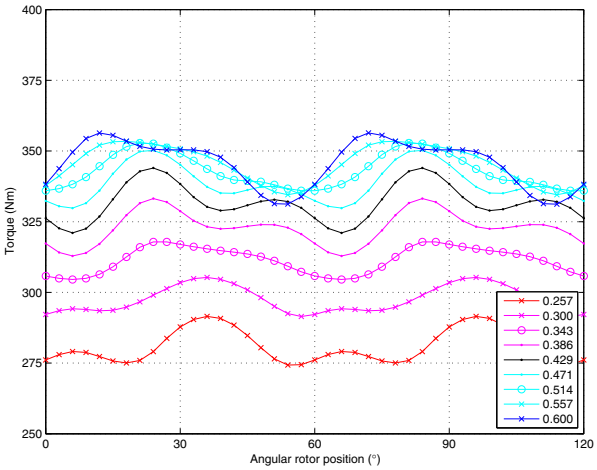

Fig. 11: Load torque with various ratios b_t/τ_s of tooth width and slot pitch, $\underline{i}_{S,dq} = \jmath$, Δ-connected stator winding

connected stator winding will generate slightly more power losses in the stator windings. Further, the latter one shows smaller mean values of the load torque with the same stator currents and more significant higher harmonic components with the cogging torque. Nevertheless, the 6th harmonic component is always less for the Δ-connected stator winding than for the Y-connected stator winding. Consequently, for the same stator currents the first one produces a smoother load torque along the circumferential direction.

V. Conclusion

The paper discusses parametric finite element analyses of an external rotor PMSM with either a Y- or Δ-connected stator winding. In order to obtain an optimized machine design in terms of cogging torque and magnetic saliency, electromagnetic torque and no-load voltages in dependence on the angular rotor position based on geometry variations are shown in detail. As the cogging torque of the PMSM is one of the most important criterion for an application in a high performance drive system for an electric vehicle, detailed investigations concerning both Y- and Δ-connected stator windings are carried out. Consequently, an optimization of the machine design can be carried out in the design stage without a prototype of the machine.

TABLE V
Load and Cogging Torque Harmonics (Magnitudes) with Various Ratios of Tooth Width and Slot Pitch, Y-connected Stator Winding

Ratio	Load Torque (Nm)			Cogging Torque (Nm)	
b_t/τ_s	Average	6th order	12th order	6th order	12th order
0.257	289.2	5.3	3.7	0.0	7.4
0.300	306.4	5.6	1.5	0.0	4.3
0.343	321.1	6.4	2.3	0.0	0.1
0.386	333.3	7.5	4.9	0.0	4.1
(ID) 0.429	343.2	8.9	5.8	0.0	6.3
0.471	350.9	10.5	4.3	0.0	5.9
0.514	356.4	12.2	1.2	0.0	3.2
0.557	359.8	13.8	2.3	0.0	0.5
0.600	361.1	15.2	4.7	0.0	3.8

TABLE VI
Load and Cogging Torque Harmonics (Magnitudes) with Various Ratios of Tooth Width and Slot Pitch, Δ-connected Stator Winding

Ratio	Load Torque (Nm)			Cogging Torque (Nm)	
b_t/τ_s	Average	6th order	12th order	6th order	12th order
0.257	280.9	6.8	4.6	9.9	6.6
0.300	297.6	6.2	2.0	8.8	3.6
0.343	311.6	6.1	1.9	7.6	0.6
0.386	322.9	6.2	5.2	6.5	4.5
(ID) 0.429	331.9	6.5	6.5	5.4	6.6
0.471	338.7	7.1	5.3	4.4	6.2
0.514	343.1	8.0	2.3	3.5	3.4
0.557	345.5	9.0	2.1	2.6	0.6
0.600	345.8	10.2	5.1	1.8	4.0

References

[1] Huth G.: "Permanent Magnet Excited AC Servo Motors in Tooth Coil Technology". *IEEE Transactions on Energy Conversion*, Vol. 20, No. 2, June 2005.

[2] El-Refaie A.M., Shah M.R.: "Comparison of Induction Machine Performance with Distributed and Fractional-Slot Concentrated Windings". *IEEE Industry Applications Society Annual Meeting, IAS*, Edmonton (AB, Canada), October 2008.

[3] Bianchi N., Fornasiero E.: "Impact of MMF Space Harmonic on Rotor Losses in Fractional-Slot Permanent-Magnet Machines". *IEEE Transactions on Energy Conversion*, Vol. 24, No. 2, June 2009.

[4] El-Refaie A.M.: "Fractional Slot Concentrated Windings Synchronous Permanent Magnet Machines: Opportunities and Challenges". *IEEE Transactions on Industrial Electronics*, Vol. 57, No. 1, January 2010.

[5] Schmidt E.: "Comparison of Different Designs of Normal and Permanent Magnet Excited Reluctance Machines". *Proceedings of the 9th International Conference on Modeling and Simulation of Electrical Machines, Converters and Systems, ELECTRIMACS*, Quebec City (QC, Canada), 2008.

[6] Schmidt E., Eilenberger A.: "Calculation of Position Dependent Inductances of a Permanent Magnet Synchronous Machine with an External Rotor by using Voltage Driven Finite Element Analyses". *IEEE Transactions on Magnetics*, Vol. 45, No. 3, March 2009.

[7] Jin J.: *The Finite Element Method in Electromagnetics*. John Wiley & Sons, New York (USA), 2002.

[8] Bastos J.P.A., Sadowski N.: *Electromagnetic Modeling by Finite Element Methods*. Marcel Dekker Ltd, New York (USA), 2003.

[9] De Gersem H., Mertens R., Lahaye D., Vandewalle S., Hameyer K.: "Solution Strategies for Transient, Field-Circuit Coupled Systems". *IEEE Transactions on Magnetics*, Vol. 36, No. 4, July 2000.

[10] De Gersem H., Gyselinck J., Dular P., Hameyer K., Weiland T.: "Comparison of Sliding Surface and Moving Band Techniques in Frequency-Domain Finite Element Models of Rotating Machines". *Proceedings of the 6th International Workshop on Electric and Magnetic Fields, EMF*, Aachen (Germany), 2003.

[11] De Gersem H., Weiland T.: "Harmonic Weighting Functions at the Sliding Surface Interface of a Finite Element Machine Model Incorporating Angular Displacement". *IEEE Transactions on Magnetics*, Vol. 40, No. 2, March 2004.

[12] Park R.H.: "Two-Reaction Theory of Synchronous Machines, Generalized Method of Analysis". *AIEE Transactions*, Part. I, Vol. 48, July 1929.

[13] Kovacs P.K.: *Transient Phenomena in Electrical Machines*. Elsevier, Amsterdam, 1984.

Erich Schmidt was born in Vienna, Austria, in 1959. He received his MSc and PhD degrees in Electrical Engineering from the Vienna University of Technology, Austria, in 1985 and 1993, respectively. Currently, he is an Associate Professor of Electrical Machines at the Institute of Electrical Drives and Machines of the Vienna University of Technology. His research and teaching activities are on numerical field computation techniques and design optimization of electrical machines and transformers. He has authored more than 100 technical publications mainly in the fields of electrical machines and numerical field calculation.

Marko Sušić was born in Klagenfurt, Austria, in 1980. He received his BSc and MSc degrees in Electrical Engineering from the Vienna University of Technology, Austria, in 2008 and 2010, respectively. Currently, he is with the scientific staff at the Institute of Electrical Drives and Machines of the Vienna University of Technology and works on finite element analyses of permanent magnet synchronous machines.

Andreas Eilenberger was born in Vienna, Austria, in 1980. He received his BSc and MSc degrees in Electrical Engineering from the Vienna University of Technology, Austria, in 2004 and 2006, respectively. Afterwards, he joined the scientific staff at the Institute of Electrical Drives and Machines of the Vienna University of Technology. Currently, he works toward his PhD thesis on sensorless control of permanent magnet synchronous machines.